Available online at www.sciencedirect.com
SCIENCE DIRECT®
International Journal of Heat and Mass Transfer 47 (2004) 2577–2586
International Journal of HEAT and MASS TRANSFER
www.elsevier.com/locate/ijhmt

Inverted fins: geometric optimization of the intrusion into a conducting wall

C. Biserni [a,*], L.A.O. Rocha [b], A. Bejan [c]

[a] Dipartimento di Ingegneria Energetica, Nucleare e del Controllo Ambientale, Università degli Studi di Bologna, Viale Risorgimento 2, 40136 Bologna, Italy

[b] Departamento de Física, Fundação Universidade Federal, de Rio Grande, Av. Itália, Km 8, CP-474, Rio Grande, RS 96201-900, Brazil

[c] Department of Mechanical Engineering and Materials Science, Duke University, Box 90300, Durham, NC 27708-0300, USA

Received 18 September 2003; received in revised form 22 December 2003

Abstract

In this paper we consider the optimization of the shape of a cavity that intrudes into a solid conducting wall. This intrusion may be regarded as a "negative fin", i.e., the outside-in version of a conductive fin the shape of which is to be optimized. The objective is to minimize the global thermal resistance between the solid and the cavity. The cavity is rectangular, with fixed volume and variable aspect ratio. The cavity shape is optimized for two sets of thermal conditions for the solid wall: uniform heat generation, and uniform heat flux on the outer surfaces of the solid wall. The optimized cavity shape is practically independent of the thermal conditions. The cavity shape is optimal when it penetrates the conducting wall completely. In the second part of the paper we optimized a more complex intrusion: a cavity shaped as a T. The performance of the T-shaped cavity is superior to that of the finger-shaped cavity optimized in the first part of the paper.

1. Introduction

Constructal theory and design [1] serves as a reminder that flow systems that must be designed (configured) must be treated as malleable, i.e., as morphing structures that are as free to change as possible. Configurations that are postulated (assumed) based on past practice, handbooks and rules of thumb, are not necessarily the best. The only rule of thumb worth remembering is that geometry must not be taken for granted. Geometry matters, in fact, geometry is the result, not an assumption. It is geometry that endows the flow system with the ability to serve its purpose, in spite of the constraints.

The field of heat transfer has demonstrated for many years how the principle of generating flow geometry works. The oldest and most clear illustrations are the optimization of solid wall features known as extended surfaces, or fins. The most recent treatise on this subject [2] recounts not only the optimization of the shapes of individual fins, but also the optimization of the architecture of assemblies of fins, e.g., finned heat sinks, bushes and trees of fins, as well as leaf-like fins with toothy edges [3]. Many more examples are found in the growing volume of techniques for the cooling of compact and miniaturized packages of electronics [4–6].

In this paper we consider the constructal design of another, equally basic feature of a solid wall with heat transfer: the open cavity. This is the "negative fin", or the outside-in version of the solid fin geometry. It is as basic as the solid fin itself, because it is found in practically every domain where augmentation and compactness (high density) of heat transfer are required.

For example, open cavities are the regions formed between adjacent fins. If the optimization of the geometry of the individual fin is an important issue, then, certainly, the geometry of the interstices must also be

* Corresponding author. Tel.: +39-05120-93292; fax: +39-05120-93296.
E-mail address: cesare.biserni@unibo.it (C. Biserni).

0017-9310/$ - see front matter © 2004 Elsevier Ltd. All rights reserved.
doi:10.1016/j.ijheatmasstransfer.2003.12.018

Nomenclature

A	area, $A = HL$, m^2
D_0	elemental thickness, m
D_1	stem thickness, m
H	height, m
H_0	cavity height, m
j	mesh index
k	solid thermal conductivity, $W\,m^{-1}\,K^{-1}$
L	length, m
L_0	elemental length, m
L_1	stem length, m
$N_{x,y}$	number of grid points
q	heat current, W
q''	heat flux, $W\,m^{-2}$
q'''	heat generation rate per unit volume, $W\,m^{-3}$
T	temperature, K
V	volume, m^3
V_0	cavity volume, m^3
W	width, m
x, y	cartesian coordinates, m

Greek symbols

ϕ	volume fraction occupied by the cavity
ψ	volume fraction occupied by the rectangular territory defined by the T-shaped structure

Superscripts

$(\tilde{})$	dimensionless variables, Eqs. (5)–(7)
$(\hat{})$	dimensionless variable, Eq. (13)

Subscripts

max	maximum
min	minimum
opt	optimum
ref	reference

important. Open cavities are essential promoters of nucleate boiling and condensation: see, for example, the vapotron effect [7–13]. Open cavities are important morphological features in physiology. The alveolus of the lung is a very good example, where the relatively robust (not slender) shape of the cavity has been noted and attributed intuitively to the natural constructal optimization principle (Ref. [1], p. 102).

In this paper we consider the optimization of the cavity shape in the most fundamental sense, without application to a particular device or field. We rely on the constructal method: the cavity shape is free to change subject to volume constraints, and in the pursuit of maximal global performance. The global performance indicator is the overall thermal resistance between the volume of the entire system (cavity and solid) and the surroundings. For simplicity and clarity, we consider two-dimensional geometries where the overall volume and the cavity volume are rectangles with variable geometric aspect ratios.

2. Body with heat generation

Consider the two-dimensional C-shaped conducting body shown in Fig. 1. The external dimensions (H, L) vary. The third dimension, W, is perpendicular to the plane of the figure. The total volume occupied by this body is fixed,

$$V = HLW \tag{1}$$

Alternatively, the area $A = HL$ is fixed. The dimensions of the cavity (H_0, L_0) also vary. The cavity volume is fixed,

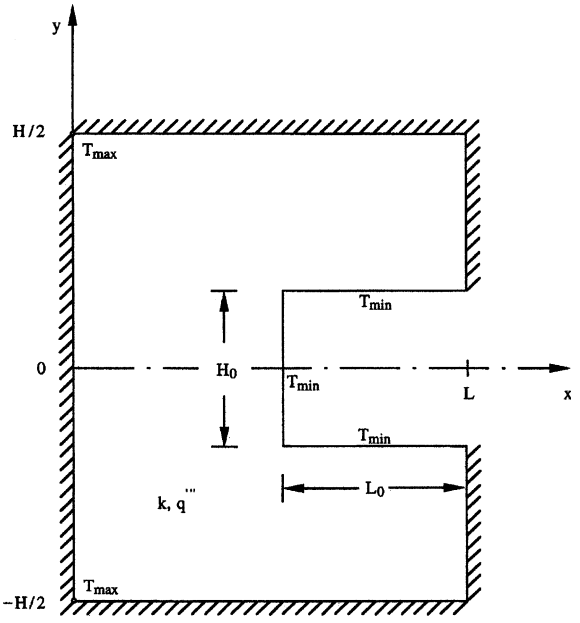

Fig. 1. Isothermal lateral intrusion into a two-dimensional conducting body with uniform heat generation.

$$V_0 = H_0 L_0 W \tag{2}$$

The constant volume constraint is justified in many applications: the cost of material and the weight and space of the heat transfer device make this constraint indispensable in design work. In constructal design, this constraint is part of the mechanism of generating the optimal geometric form that fills a given space. This

constraint may be replaced by the statement that the volume fraction occupied by the cavity is fixed,

$$\phi = \frac{V_0}{V} = \frac{H_0 L_0}{HL} \tag{3}$$

The solid is isotropic with the constant thermal conductivity k. It generates heat uniformly at the volumetric rate q''' (W/m^3). The outer surfaces of the heat generating body are perfectly insulated. The generated heat current ($q'''A$) is removed by cooling the wall of the cavity. The cavity wall temperature is maintained at $T_{\min}$. Temperatures in the solid are higher than $T_{\min}$. The highest temperatures (the "hot spots") are registered at points on the adiabatic perimeter, for example, in the two corners indicated with $T_{\max}$ in Fig. 1.

The isothermal cavity wall assumption is made for simplicity in demonstrating the construction of optimal cavity shape. This assumption means that the heat transfer coefficient on the internal (exposed) surface of the cavity is sufficiently large, so that wall conduction poses a larger thermal resistance than convection. This assumption can be relaxed in future applications of this construction method, as is discussed later in Section 6. In a more realistic model, the cavity wall temperature and heat flux would be related, and the wall temperature distribution would vary with the shape of the cavity.

An important thermal design constraint is the requirement that temperatures must not exceed a certain level. This makes $T_{\max}$ a constraint. The design also calls for installing a maximum of heat generation rate in the fixed volume, which corresponds to packing the most electronics into a device of fixed size. In the present problem statement, this design objective is represented by the maximization of the global thermal conductance $q'''A/(T_{\max} - T_{\min})$, or by the minimization of the global thermal resistance $(T_{\max} - T_{\min})/(q'''A)$.

The numerical optimization of geometry consisted of simulating the temperature field in a large number of configurations, calculating the global thermal resistance for each configuration, and selecting the configuration with the smallest global resistance. Symmetry allowed us to perform calculations in only half of the domain, $y \geqslant 0$. The conduction equation for the solid region is

$$\frac{\partial^2 \widetilde{T}}{\partial \tilde{x}^2} + \frac{\partial^2 \widetilde{T}}{\partial \tilde{y}^2} + 1 = 0 \tag{4}$$

Table 1
Numerical tests showing the achievement of grid independence ($H/L = 1$, $\phi = 0.1$, $H_0/L_0 = 0.4$)

N_x	N_y	$\widetilde{T}_{\max}$	$\lvert(\widetilde{T}^j_{\max} - \widetilde{T}^{j+1}_{\max})/\widetilde{T}^j_{\max}\rvert$
17	17	0.218845	2.17026×10^{-3}
33	33	0.219320	8.49444×10^{-4}
65	65	0.219506	3.33977×10^{-4}
129	129	0.219579	

where the dimensionless variables are

$$\widetilde{T} = \frac{T - T_{\min}}{q'''A/k} \tag{5}$$

$$\left(\tilde{x}, \tilde{y}, \widetilde{H}, \widetilde{L}, \widetilde{H}_0, \widetilde{L}_0\right) = \frac{(x, y, H, L, H_0, L_0)}{A^{1/2}} \tag{6}$$

The boundary conditions are indicated in Fig. 1. The maximal excess temperature, $\widetilde{T}_{\max}$, is also the dimensionless global thermal resistance of the construct,

$$\widetilde{T}_{\max} = \frac{T_{\max} - T_{\min}}{q'''A/k} \tag{7}$$

It is not possible to express the global objective function $\widetilde{T}_{\max}$ in analytical form, in terms of the geometric parameters of the cavity. This function can be determined numerically, by solving for the temperature field in every assumed configuration, and the calculating $\widetilde{T}_{\max}$ to see whether $\widetilde{T}_{\max}$ can be minimized by varying the configuration.

Eq. (4) was solved using a finite elements code [14] based on quadrilateral elements and biquadratic interpolation functions. The grid was uniform in both $\tilde{x}$ and $\tilde{y}$, and varied from one geometry to the next. The appropriate mesh size was determined by successive refinements, until the further doubling of the number of grid points in both directions (N_x, N_y) satisfied the criterion $|(\widetilde{T}^j_{\max} - \widetilde{T}^{j+1}_{\max})/\widetilde{T}^j_{\max}| < 5 \times 10^{-4}$. Here $\widetilde{T}^j_{\max}$ represents the maximum temperature calculated using the current mesh size, and $\widetilde{T}^{j+1}_{\max}$ corresponds to the next mesh, where N_x and N_y were doubled. Table 1 gives an example of how grid independence was achieved. The following results were obtained by using $N_x = 65$ and $N_y = 65$.

The accuracy of these numerical results were tested by solving Eq. (4) using the MATLAB partial-differential-equations (pde) toolbox [15], and comparing the results with those using the FIDAP package. Table 2

Table 2
Comparison between the results obtained using the FIDAP package and the MATLAB partial-differential-equations (pde) toolbox ($H/L = 1$, $\phi = 0.3$)

H_0/L_0	$\widetilde{T}_{\max}$ (FIDAP)	$\widetilde{T}_{\max}$ (MATLAB – pde)	$\lvert(\widetilde{T}^{\text{FIDAP}}_{\max} - \widetilde{T}^{\text{MATLAB}}_{\max})/\widetilde{T}^{\text{FIDAP}}_{\max}\rvert$
1.875	0.1873	0.1873	0
1.2	0.1436	0.1435	6.964×10^{-4}
0.8334	0.10865	0.1086	4.602×10^{-4}
0.4686	0.06574	0.0657	6.085×10^{-4}

shows this comparison for several values of H_0/L_0. The two sets of results agree within 0.07%.

3. Optimization of geometry

We solved the conduction problem in many configurations $(H/L, H_0/L_0, \phi)$. Fig. 2 shows that the thermal resistance can be minimized by selecting the shape of the cavity. The thermal resistance decreases when the volume fraction (ϕ) occupied by the cavity increases. This conclusion is confirmed in Fig. 3, where the minimal global thermal resistance is shown as a function of the relative size of the cavity, ϕ. The optimal shape of the cavity is also reported.

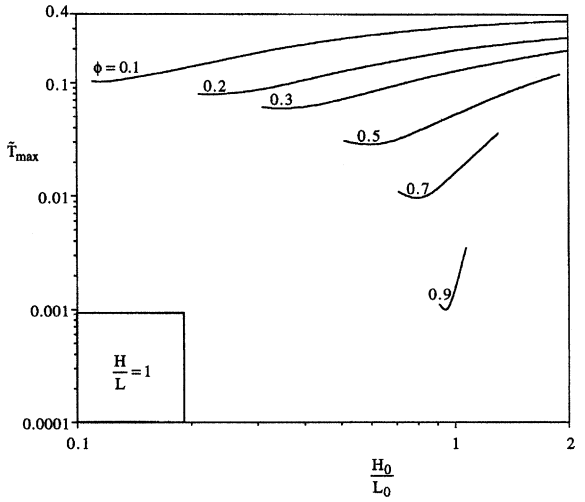

Fig. 2. The minimization of the global thermal resistance when the external shape of the heat generating body is fixed.

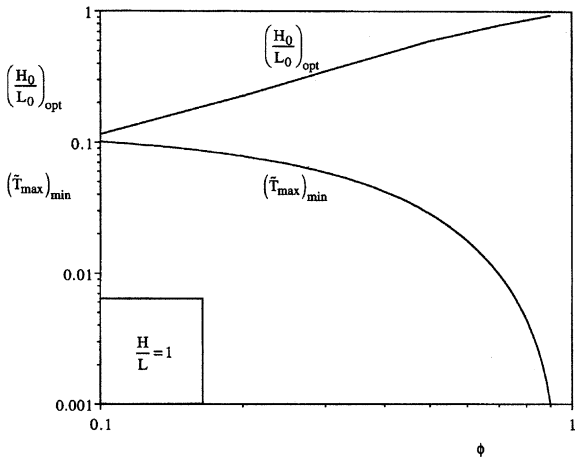

Fig. 3. The optimized geometry and performance when the external shape is square.

The second level of the numerical optimization scheme consisted of repeating the preceding work (Figs. 2 and 3) for many values of the second shape parameter, H/L. The most important finding is that an optimal H/L ratio does not exist, i.e., the geometry of Fig. 1 can be optimized only with respect to one degree of freedom.

Fig. 4 shows why a second optimization opportunity does not exist: the global resistance minimized with respect to H_0/L_0 varies monotonically with H/L. When ϕ is sufficiently small, $(\widetilde{T}_{max})_{min}$ is proportional to H/L, and the effect of ϕ on this proportionality vanishes. Performance improves as the external shape becomes slender ($H \ll L$), and as the volume occupied by the lateral intrusion (ϕ) increases.

The optimized intrusion shape that corresponds to Fig. 4 is shown in Fig. 5. The optimized internal shape

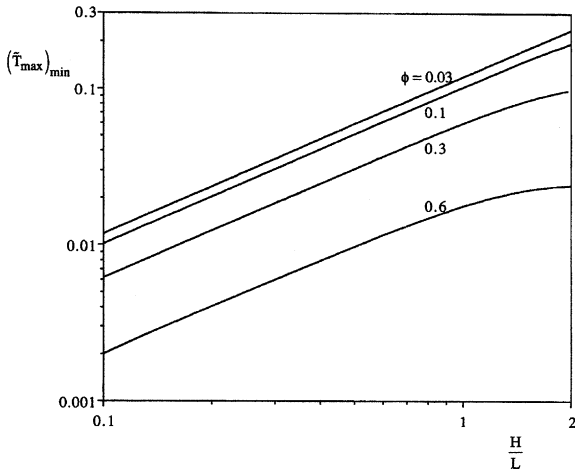

Fig. 4. The effect of the external shape H/L on the global thermal resistance minimized as in Fig. 2.

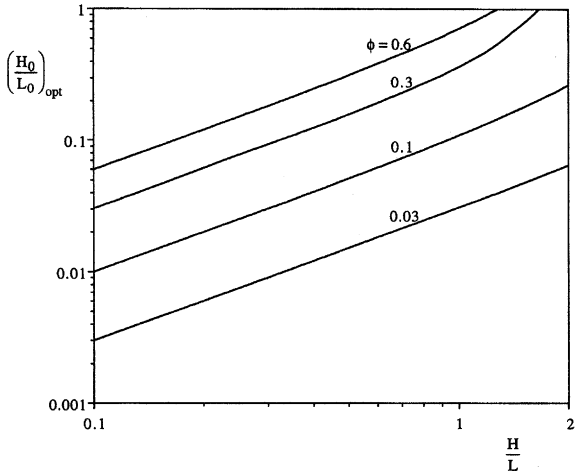

Fig. 5. The optimal shape of the lateral intrusion, as a function of H/L and ϕ.

parameter $(H_0/L_0)_{opt}$ is approximately proportional to the assumed external shape H/L, and increases with ϕ. These observations are the basis for constructing Fig. 6, which shows that when ϕ is small the effect of H/L and ϕ on $(H_0/L_0)_{opt}$ can be correlated approximately as

$$\left(\frac{H_0}{L_0}\right)_{opt} \cong \phi\frac{H}{L} \tag{8}$$

We return to this observation in Section 5.

We confirmed the validity of the results of Figs. 4–6 by reversing the order in which we varied the two shape parameters during the search for the lowest $\tilde{T}_{max}$. In other words, contrary to Figs. 4–6, we began with holding H_0/L_0 fixed and varying H/L. This first level also resulted in an optimal H/L. Fig. 7 shows that the minimal global thermal resistance and the optimal external shape of the conducting wall decrease when the volume fraction ϕ increases. At the second level of numerical work, we repeated the first-level calculations for many values of H_0/L_0. In this way we found that H_0/L_0 can be optimized, and that when $\phi \geqslant 0.3$ the results are approximately the same as in Figs. 4–6. Fig. 8 shows a comparison between the two cases, $(H/L)_{fixed}$ and $(H_0/L_0)_{fixed}$. The minimized global resistance is practically the same as in Fig. 4, especially when ϕ is greater than 0.1. When ϕ is smaller than 0.1, and when $H/L > 0.5$ the minimized global resistance is larger when H_0/L_0 is fixed than when H/L is fixed. Fig. 9 confirms that $(H/L)_{opt}$ and $(H_0/L_0)_{opt}$ are essentially the same for the two ways in which they are calculated, provided that H/L is below 0.5.

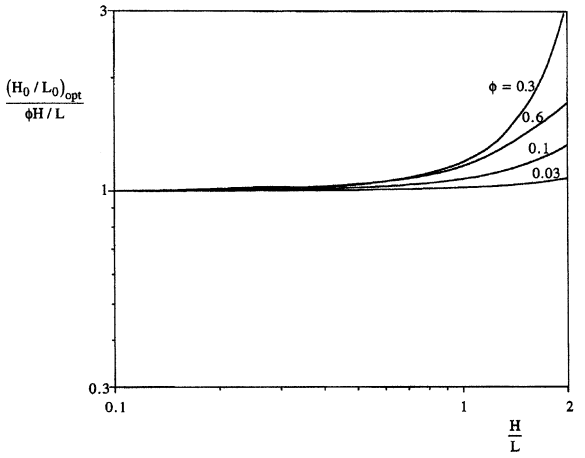

Fig. 6. Correlation of the optimal shape results of Fig. 5.

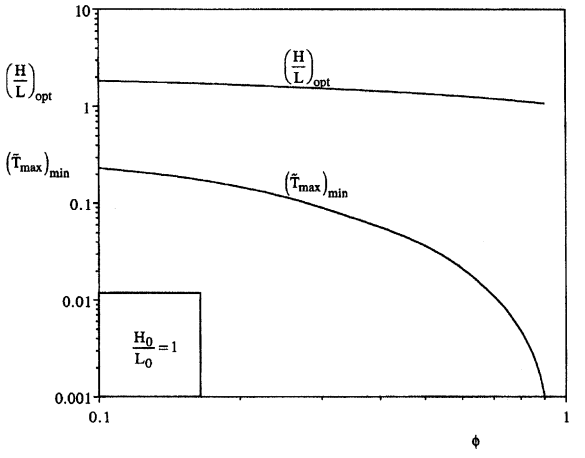

Fig. 7. The optimized geometry and performance when the internal shape is square.

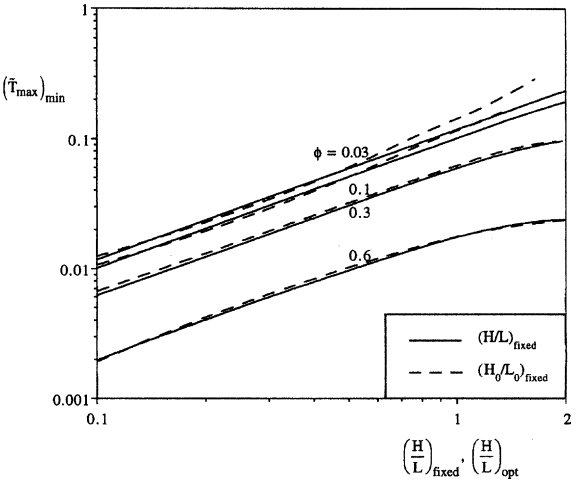

Fig. 8. The effect of the external shape H/L on the global thermal resistance minimized for constant H/L.

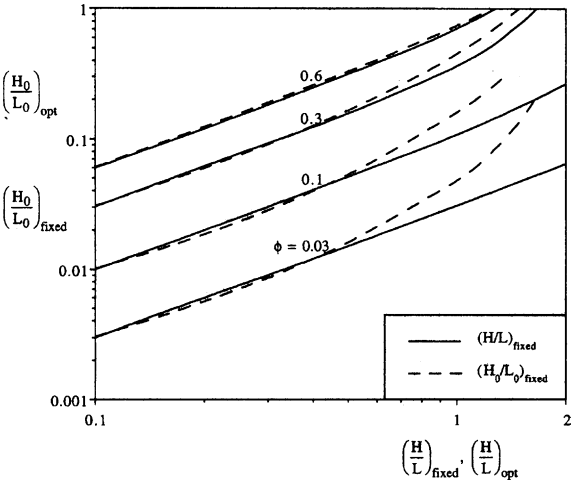

Fig. 9. The optimal shape obtained by holding H/L fixed, versus the optimal shape obtained by holding H_0/L_0 fixed.

4. Body heated externally

It is important to test the robustness of the optimized geometry. For example, is the optimal cavity shape sensitive to changes in how the solid body is heated? We explored this idea by using the heating arrangement shown in Fig. 10, and by repeating the two-level optimization documented in Figs. 2–6. The conducting body is heated with uniform heat flux (q'') over that portion of its periphery that does not come into direct contact with the $T_{\min}$ surface of the cavity. The body does not generate heat volumetrically. The total heat current is fixed,

$$q = q''(H + 2L)W \tag{9}$$

The volume constraints (1) and (3) continue to apply. Lengths continue to be nondimensionalized based on $A^{1/2}$, Eq. (6). The imposed heat current, Eq. (9), means that the heat flux q'' varies as the external shape $(\widetilde{H}, \widetilde{L})$ varies,

$$q'' = \frac{q''_{\text{ref}}}{\widetilde{H} + 2\widetilde{L}} \tag{10}$$

The reference heat flux is fixed because it is based on the total heat current, which is fixed,

$$q''_{\text{ref}} = \frac{q}{A^{1/2}W} \tag{11}$$

The conduction equation for points in the solid is

$$\frac{\partial^2 \widehat{T}}{\partial \tilde{x}^2} + \frac{\partial^2 \widehat{T}}{\partial \tilde{y}^2} = 0 \tag{12}$$

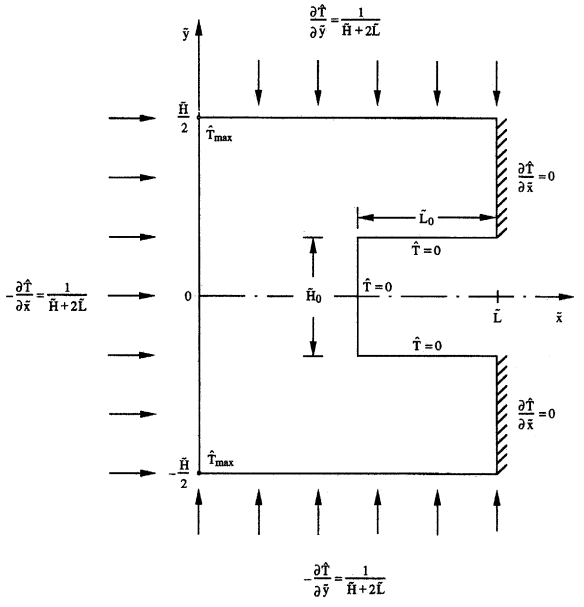

Fig. 10. Body with lateral intrusion and uniform heat flux on a portion of its external surface.

where $\widehat{T}$ is the new dimensionless temperature

$$\widehat{T} = \frac{T - T_{\min}}{q''_{\text{ref}} A^{1/2}/k} \tag{13}$$

The boundary conditions are indicated in Fig. 10, namely, $\widehat{T} = 0$ on the internal surfaces, and $\partial \widehat{T}/\partial \tilde{x} = 0$ on the shaded portions of the $\tilde{x} = \widetilde{L}$ boundary. On the $\tilde{x} = 0$ face, the boundary condition $q'' = -k(\partial T/\partial x)_0$ becomes

$$-\frac{\partial \widehat{T}}{\partial \tilde{x}} = \frac{1}{\widetilde{H} + 2\widetilde{L}} \tag{14}$$

Similarly, the uniform-q'' condition on the top side $(\tilde{y} = \widetilde{H}/2)$ reads

$$\frac{\partial \widehat{T}}{\partial \tilde{y}} = \frac{1}{\widetilde{H} + 2\widetilde{L}} \tag{15}$$

The remaining boundary condition is $\partial \widehat{T}/\partial \tilde{y} = 0$ at $\tilde{y} = 0$, or $\partial \widehat{T}/\partial \tilde{y} = -1/(\widetilde{H} + 2\widetilde{L})$ at $\tilde{y} = -\widetilde{H}/2$. The numerical method and grid refinement procedure were the same as in Section 2.

The optimization of geometry proceeded in two phases. In the first, we held H/L and optimized H_0/L_0. The minimized dimensionless hot spot temperature $(\widehat{T}_{\max})_{\min}$ defined based on Eq. (13) is reported in Fig. 11. The corresponding optimal internal aspect ratio is shown in Fig. 12. In the second phase of numerical simulation we repeated the first phase for many values of H/L, as summarized in Figs. 11 and 12. We found that the overall thermal resistance increases monotonically

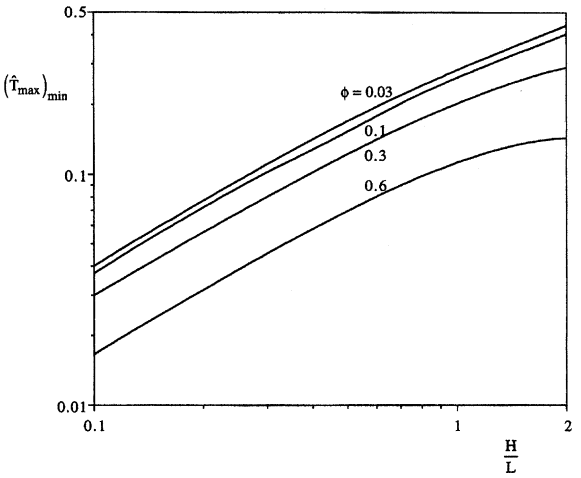

Fig. 11. The effect of the external shape on the minimized global thermal resistance when the body is heated externally.

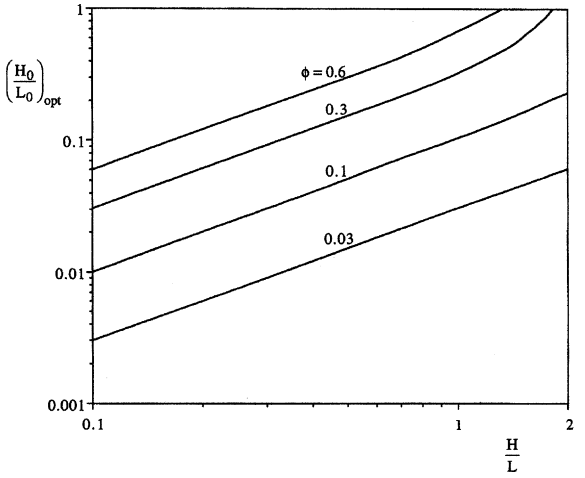

Fig. 12. The effect of the external shape on the optimal shape of the lateral intrusion when the body is heated externally.

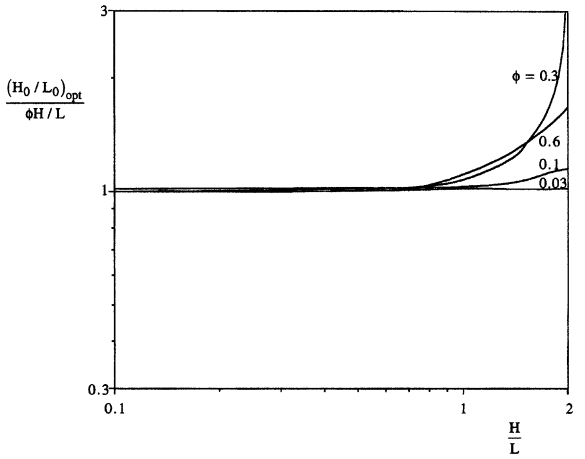

Fig. 13. Correlation of the results for the optimal internal shape when the body is heated externally.

with H/L, and that an optimal H/L does not exist when H_0/L_0 has already been optimized.

It is interesting to compare the present results (Figs. 11 and 12) with the corresponding curves for the body heated internally (Figs. 4 and 5). The trends are the same. In particular, the optimized internal aspect ratio has practically the same value in both cases. This point is made more clearly in Fig. 13, which is nearly the same as Fig. 6. The optimized geometry is indeed robust: it is relatively insensitive to how the body is heated.

5. First construct

One direction in which the optimization of intrusion geometry can be pursued is that of increasing the complexity of the growing structures, in spaces that grow as they are cooled by expanding flow structures. When the heat generated by the volume is removed through one port, and when the smallest volume element size is fixed, the optimization of geometry generates a tree-shaped flow structure [1]. The simplest tree-shaped structure is a "first construct", or an optimized assembly of elemental volumes. The simplest first construct is the T-shaped tree [16].

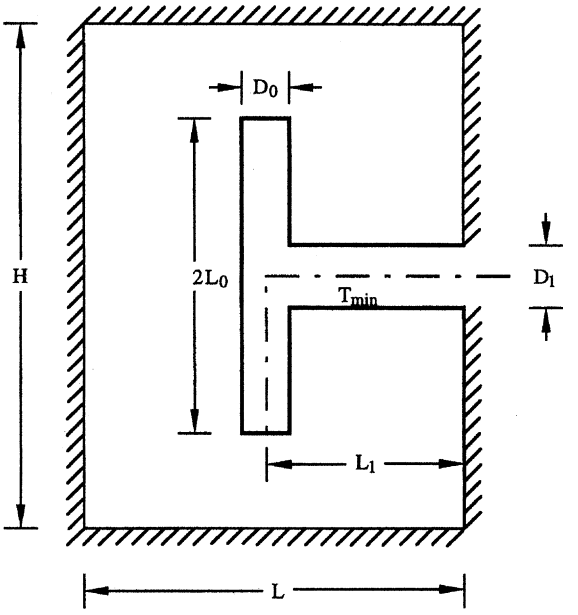

Fig. 14. First construct of intrusions arranged as a T.

Fig. 14 shows the T-shaped intrusion formed by a 'stem' intrusion ($L_1 \times D_1$) that branches into two elemental intrusions ($L_0 \times D_0$). The optimization of the elemental intrusion formed the subject of Sections 2–4. In Fig. 14, the global size of the construct ($HL = A$) is fixed. The solid material has the conductivity k and generates heat volumetrically at the uniform rate q'''. The perimeter of the HL rectangle is insulated. The surface of the cavity is isothermal at T_{min}. The hot spot of temperature T_{max} occurs at one or more points in the solid. The objective continues to be the minimization of the global thermal resistance $\tilde{T}_{max}$, which is defined the same way as in Eq. (5).

The geometry of the T-shaped construct is subjected to two constraints, the volume fraction occupied by the cavity

$$\phi = \frac{2L_0D_0 + (L_1 - D_0/2)D_1}{HL} \tag{16}$$

and the volume fraction occupied by the rectangle defined by the T,

$$\psi = \frac{2L_0(L_1 + D_0/2)}{HL} \tag{17}$$

The structure has three degrees of freedom, which are represented by the ratios H/L, L_0/L_1 and D_0/D_1. In the following sequence of optimization results we fixed $H/L = 1$, optimized L_0/L_1 by minimizing $\widetilde{T}_{max}$, and then repeated the optimization for other values of D_0/D_1.

Fig. 15 shows that the results of the optimization with respect to L_0/L_1 are practically insensitive to changes in D_0/D_1. A weak effect emerges when ϕ becomes greater than 0.1, as shown in Figs. 16 and 17. There is no optimum with respect to D_0/D_1. The mini-

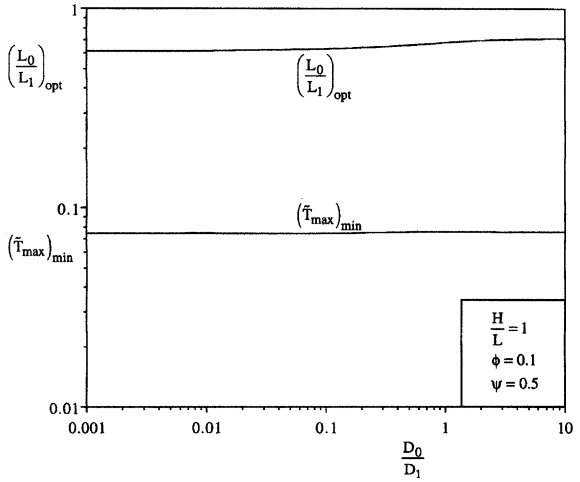

Fig. 15. The effect of the ratio D_0/D_1 on the minimized global thermal resistance, and on the optimized lengths ratio.

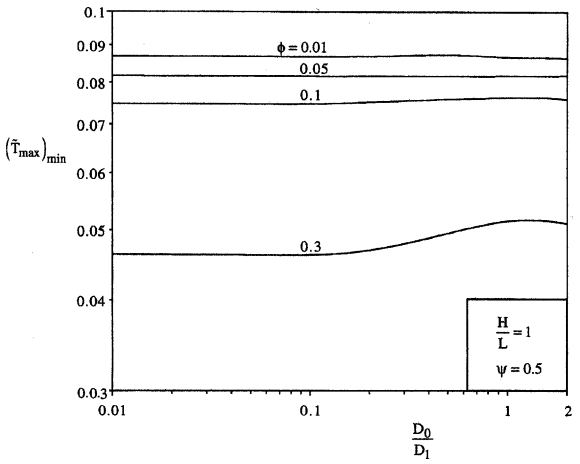

Fig. 16. The effect of the ratio D_0/D_1 and ϕ on the minimized global thermal resistance.

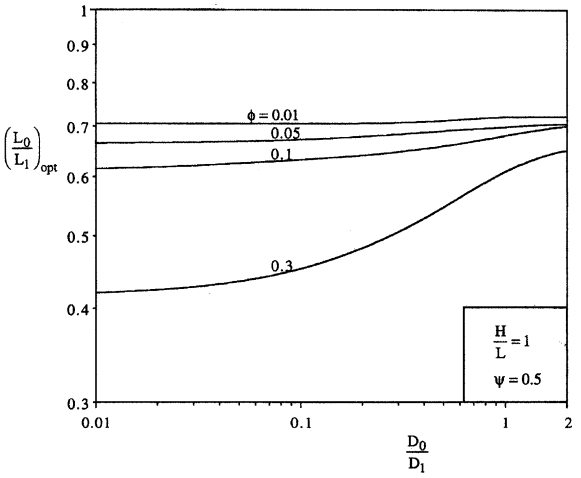

Fig. 17. The behavior of the optimized geometry as ϕ and the ratio D_0/D_1 vary.

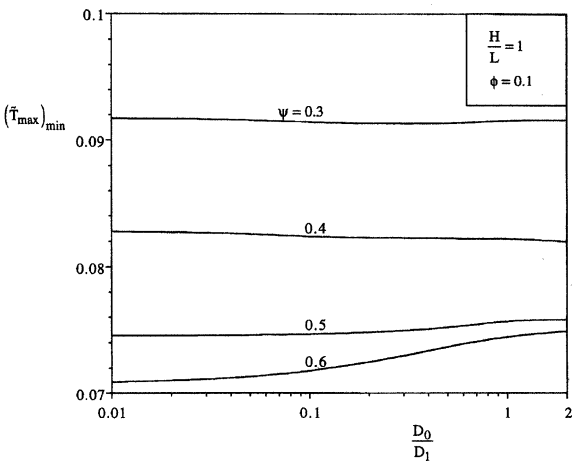

Fig. 18. The effect of ψ and D_0/D_1 on the minimized global resistance.

mized global resistance and the optimized lengths ratio decrease as ϕ increases.

Figs. 18–20 show the effect of ψ on the optimization results sampled in Fig. 14. The minimized global resistance decreases as the T-shaped cavity grows, i.e. as ψ increases (Fig. 18). At the same time, the aspect ratio $(L_0/L_1)_{opt}$ increases. This trend is presented in Figs. 19 and 20.

6. Conclusions

Several conclusions and ideas for future research emerged from this study. First is the surprisingly tight correlation of the numerical results for $(H_0/L_0)_{opt}$,

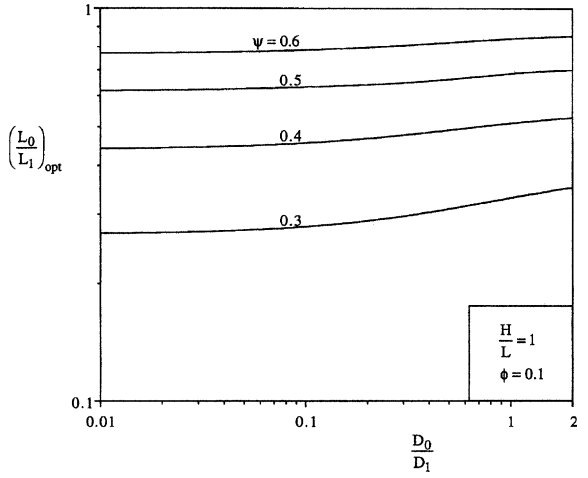

Fig. 19. The behavior of the ratio $(L_0/L_1)_{\text{opt}}$ when ψ and D_0/D_1 change.

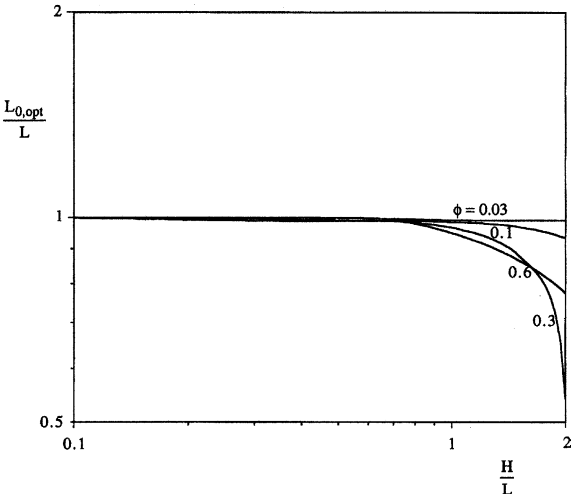

Fig. 21. The optimal penetration distance of the lateral intrusion.

cf. Figs. 6 and 13. We found based on pure observation that the $(H_0/L_0)_{\text{values}}$ are such that the group shown on the ordinate of Figs. 6 and 13 is equal to 1 when ϕ is of order 0.1 or smaller,

$$\frac{(H_0/L_0)_{\text{opt}}}{\phi H/L} \sim 1 \tag{18}$$

Because $\phi = H_0L_0/(HL)$, this correlation is the same as

$$\left(\frac{L}{L_0}\right)^2 \sim 1 \tag{19}$$

Fig. 21 shows that correlation (19) is valid when the external aspect ratio of the conducting body is $H/L < 1$. The lateral cavity reaches its best shape when it penetrates the body almost completely. This conclusion is valid for both configurations, internal heating (Fig. 1) and external heating (Fig. 10). Future work may extend this investigation to the more general case where the heat transfer on the internal surface of the cavity is accounted for by a constant heat transfer coefficient, that is by a proportionality between the heat flux and the temperature difference between the cavity wall and the fluid that bathes the cavity.

We can compare the performance of the elemental volume showed in Fig. 1 with the performance of the first construct drawn in Fig. 14 under the same thermal conditions, uniform heat generation, and the same volume fraction occupied by the cavity, ϕ. Fig. 2 shows the behavior of the global thermal resistance, $\widetilde{T}_{\max}$, when the external shape of the body is squared, $H/L = 1$, and $\phi = 0.1$. Fig. 18 illustrates that the T-shaped configuration, the more complex one, performs better than the finger-shaped cavity of Fig. 2. This means that its minimized global thermal resistance is smaller than the one shown in Fig. 2. This performance improves when ψ increases, i.e., when the T-shaped cavity has more freedom to vary. The best T-shaped cavity configuration performs approximately 29% better than the best finger-shaped configuration.

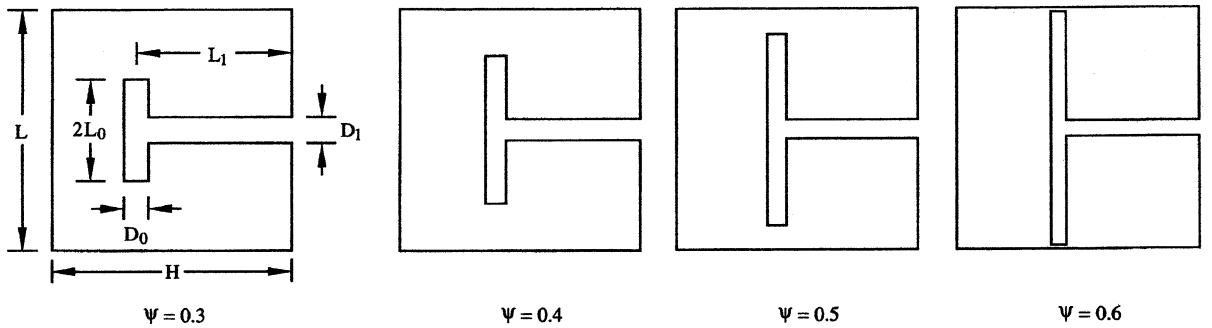

Fig. 20. The optimal configurations obtained when $D_0/D_1 = 1$, $\phi = 0.1$, and ψ varies from 0.3 to 0.6.

Acknowledgements

Dr. Cesare Biserni's work was supported by MIUR and CNR, Italy. Prof. Luiz Rocha's doctoral studies at Duke University were sponsored by CAPES, Brasilia, Brazil.

References

[1] A. Bejan, Shape and Structure, from Engineering to Nature, Cambridge University Press, Cambridge, UK, 2000.
[2] A.D. Kraus, A. Aziz, J. Welty, Extended Surface Heat Transfer, Wiley, New York, 2001.
[3] A.D. Snider, A.D. Kraus, The quest for the optimal longitudinal fin profile, ASME HTD 64 (1986) 43–48.
[4] G.P. Peterson, A. Ortega, Thermal control of electronic equipment and devices, Adv. Heat Transfer 20 (1990) 181–314.
[5] S.J. Kim, S.W. Lee, Air Cooling Technology for Electronic Equipment, CRC Press, Boca Raton, FL, 1995.
[6] A. Bar-Cohen, A.D. Kraus, Advances in Thermal Modeling of Electronic Components and Systems, vol. 4, ASME Press Series, 1998.
[7] C.A. Beurtheret, Les processus de vaporisation et le vapotron, Journées de la Transmission de la Chaleur, Paris, 1961.
[8] C. Biserni, G. Lorenzini, C.M. Orlandelli, Frequency analysis of the vapotron effect in forced convection: a challenge for numerical description of multiphase flows, in: First International Conference on Computational Methods in Multiphase Flow, Multiphase Flow 2001, Orlando, FL, March 2001, WIT Press, 2001, pp. 173–182.
[9] C. Biserni, G. Lorenzini, Experimental tests on subcooled boiling heat transfer under forced convection conditions, J. Eng. Thermophys. 11 (2002) 73–81.
[10] E. Lorenzini, C. Biserni, A subcooled boiling experimental application for finned surfaces cooling, in: Heat Transfer 2002, Seventh International Conference on Advanced Computational Methods in Heat Transfer, Halkidiki, Greece, 22–24 April 2002, pp. 215–221.
[11] C. Biserni, G. Lorenzini, A vapotron effect industrial application for finned surfaces cooling, in: Eighth International ANIMP Conference on Multiphase Flow in Industrial Plants, Alba, Cuneo, 18–20 September 2002, pp. 316–326.
[12] G. Cattadori, G.P. Gaspari, G.P. Celata, M. Cumo, A. Mariani, G. Zummo, Hypervapotron technique in subcooled flow boiling CHF, Exp. Thermal Fluid Sci. 7 (1993) 230–240.
[13] H.D. Falter, E. Thompson, Performance of hypervapotron beam-stopping elements at jet, Fusion Technol. 29 (1996) 584–594.
[14] FIDAP, Theory Manual, 1998, v. 8.6, Fluent, Inc.
[15] MATLAB, User's Guide, Version 6.0.088, release 12, 2000, The Mathworks, Inc.
[16] A. Bejan, L.A.O. Rocha, S. Lorente, Thermodynamic optimization of geometry: T and Y-shaped constructs of fluid streams, Int. J. Thermal Sci. 39 (2002) 949–960.